

Normal state ^{17}O NMR studies of Sr_2RuO_4 under uniaxial stress

Yongkang Luo^{1,7,*}, P. Guzman¹, A. P. Dioguardi², A. Pustogov¹, S. M. Thomas², F. Ronning², N. Kikugawa³, D. Sokolov⁴, F. Jerzembeck⁴, A. P. Mackenzie^{4,5}, C. W. Hicks⁴, E. D. Bauer², I. I. Mazin⁶, and S. E. Brown^{1†}

¹*Department of Physics & Astronomy, UCLA, Los Angeles, CA 90095, USA;*

²*Los Alamos National Laboratory, Los Alamos, New Mexico 87545, USA;*

³*National Institute for Materials Science, Tsukuba 305-0003, Japan;*

⁴*Max Planck Institute for Chemical Physics of Solids, Dresden 01187, Germany;*

⁵*Scottish Universities Physics Alliance, School of Physics and Astronomy, University of St Andrews, North Haugh, St Andrews KY16 9SS, UK;*

⁶*Code 6393, Naval Research Laboratory, Washington, DC 20375, USA; and*

⁷*Wuhan National High Magnetic Field Center and School of Physics, Huazhong University of Science and Technology, Wuhan 430074, China.*

(Dated: January 8, 2023)

The effects of uniaxial compressive stress on the normal state ^{17}O nuclear magnetic resonance properties of the unconventional superconductor Sr_2RuO_4 are reported. The paramagnetic shifts of both planar and apical oxygen sites show pronounced anomalies near the nominal \mathbf{a} -axis strain $\varepsilon_{aa} \equiv \varepsilon_v$, that maximizes the superconducting transition temperature, T_c . The spin susceptibility weakly increases on lowering the temperature below $T \simeq 10$ K, consistent with an interpretation based on the passing of a van Hove singularity through the Fermi energy. Although such a Lifshitz transition occurs in the γ band, formed by the Ru d_{xy} states hybridized with in-plane O p_{\perp} orbitals, the large Hund's coupling renormalizes the uniform spin susceptibility, which, in turn, affects the hyperfine fields of all nuclei. We estimate this "Stoner" renormalization, S , by combining the data with first-principles calculations and conclude that this is an important part of the strain effect, with implications for superconductivity.

I. INTRODUCTION

The physics of the superconducting state of Sr_2RuO_4 [1] remains a subject of longstanding importance, with particular focus on order-parameter symmetry [2]. There are numerous experimental results consistent with a chiral p -wave superconducting state [3–6], including evidence for time-reversal symmetry breaking for $T < T_c$ [7, 8], and lack of suppression of the in-plane spin susceptibility on cooling through the superconducting critical temperature T_c , as deduced from nuclear magnetic resonance (NMR) spectroscopy [9, 10] and neutron scattering [11]. At the same time, there are other experimental results inconsistent with that interpretation [12–16], and the out-of-plane spin susceptibility also remains constant [10], in contradiction with the expectations for the chiral state [5, 17].

For several reasons, the normal state physics of Sr_2RuO_4 is equally topical. It was anticipated at a very early stage that electron-electron interactions are controlled by the Hund's rule coupling [18], and it was later shown within the dynamical mean field theory that the electrons are subject to strong Hund's rule correlations while the system remains metallic and far from the Mott insulator regime [19, 20]. Mean-field Density Functional (DFT) calculations within the Generalized Gradient Approximation (GGA) are unstable against ferromagnetism [17]. Even though strong correlations lead to fluctuations suppressing this instability, there still remains a substantial Stoner renormalization of the uniform spin susceptibility. This led to the analogy with the triplet super-

fluidity of ^3He [18], anticipated earlier on the grounds that a related compound, SrRuO_3 is ferromagnetic [2]. Although later it was found that the leading magnetic instability is at a non-zero momentum $\mathbf{q}_0 \approx (\pm 0.3, \pm 0.3, 0)2\pi/a$ [21, 22], the proximity to a ferromagnetic state dominates the debate related to the superconducting order parameter symmetry [6, 23].

An additional feature is the proximity to a 2D Lifshitz point [24] associated with a van Hove singularity (vHs). Recently, striking physical property changes, including a factor of 2.5 increase in superconducting critical temperature T_c , from 1.4 K to 3.5 K [25], accompanied by a pronounced non-Fermi Liquid behavior of the resistivity [26], were observed under application of in-plane strain ε_{aa} . This was tentatively interpreted as a Fermi level crossing of the vHs when ε_{aa} reaches a critical value ε_v . Since direct experimental evidence is still lacking, it is important to test this interpretation in complementary studies of the normal state while subject to strain. Also, the vHs is expected to affect quite differently the triplet and singlet superconducting states, and this provides further motivation for physical property studies under strain. For singlet pairing, the order parameter (gap) can be large at the vHs (*e.g.*, for the $d_{x^2-y^2}$ symmetry), and thus the local density of states (DOS) enhancement at the vHs is very beneficial. On the contrary, the triplet order parameter at precisely the Lifshitz point is zero by symmetry, and therefore a triplet state is less suited to take advantage of the vHs unless the pairing interaction itself is enhanced. The latter can be possible as the DOS enhancement may bring the system closer to ferromag-

netism [27].

With these issues in mind, we set out to verify experimentally that the same strain at which T_c and Stoner factor S peak indeed corresponds to the maximum in DOS, and to assess, as quantitatively as possible, the change in DOS and Stoner enhancements to the susceptibility under strained conditions. To this end, NMR measurements inform on the details of the normal state, though site and orbitally specific hyperfine couplings. Indeed, the enhancement is evident in the results presented, and moreover, the inferred enhancement semi-quantitatively accounts for the transport results in Ref. [26]. Looking ahead, it is worth emphasizing that the method is considered a litmus test for the superconducting state parity [9, 28], including any strain-induced order-parameter changes. The results presented in the next sections are normal state ^{17}O NMR spectroscopy for in-plane $\mathbf{B} \parallel \mathbf{b}$, and out-of-plane $\mathbf{B} \parallel \mathbf{c}$ fields, as well as ^{17}O NMR relaxation rates for $\mathbf{B} \parallel \mathbf{b}$. These are interpreted by way of complementary DFT calculations.

II. EXPERIMENTAL DETAILS

Single crystalline Sr_2RuO_4 used for these measurements was grown by the floating-zone method [1]. Smaller pieces were cut and polished along crystallographic axes with typical dimensions $3 \times 0.3 \times 0.15 \text{ mm}^3$, and with the longest dimension aligned with the \mathbf{a} -axis. ^{17}O isotope ($^{17}I = 5/2$, gyromagnetic ratio $^{17}\gamma = -5.7719 \text{ MHz/T}$ [29]) spin-labelling was achieved by annealing in 50% ^{17}O -enriched oxygen atmosphere at $1050 \text{ }^\circ\text{C}$ for 2 weeks [9, 30]. The sample quality was not observably changed following this procedure, with $T_c \approx 1.44 \text{ K}$ identified by specific heat measurements (Supplemental Materials, SM) [31]. For the NMR experiments, the sample was mounted on a piezoelectric strain cell (Razorbill, UK) with an effective (exposed) length $L_0 \sim 1 \text{ mm}$ (see Fig. S1a, SM). Three samples (labeled as S1, S2 and S3) were measured in this work. A nominal compressive stress is applied along the \mathbf{a} -axis, with corresponding strains ($\varepsilon_{aa} \equiv \delta L/L_0$) estimated to be up to -0.72% using a pre-calibrated capacitive dilatometer; the accuracy is limited by the unknown deformations of the epoxy clamp [32]. For reference, the observed maximum $T_c(\varepsilon_{aa})$ occurs at a quantitatively similar displacement as reported in Ref. [25], $T_c^{max} = T_c(\varepsilon_v)$, with $\varepsilon_v \simeq -0.6\%$. Most of the NMR measurements were performed at fixed temperature $T=4.3 \text{ K}$ (and variations around it) and carrier frequency $f_0=46.8 \text{ MHz}$ ($B \simeq 8.1 \text{ T}$), using a standard Hahn echo sequence. Spectra, including satellite transitions, were collected in field-sweep mode, whereas a close examination of the central transition ($-1/2 \leftrightarrow 1/2$) for both in-plane and apical sites was carried out under fixed-field conditions. Some field and temperature dependence was explored. The application of NMR in

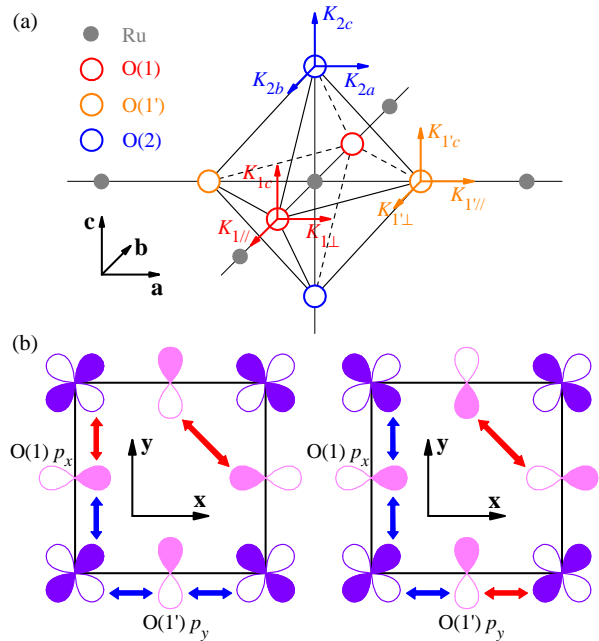


FIG. 1. (a) Configurations of planar O(1) and O(1') in RuO_2 plane and apical O(2) in the SrO layer around Ru ion in a unit cell of Sr_2RuO_4 . Compressive strain is applied along the \mathbf{a} -axis (ε_{aa}); magnetic fields are applied orthogonal, $\parallel \mathbf{b}$, $\parallel \mathbf{c}$. Arrows signify the principal axes of Knight shift tensors. (b) Orbitals forming the γ band at the X (left) and Y (right) points in the Brillouin zone. The blue (red) double-arrows show positive (negative) signs of orbital overlaps. Note that at the Y point only O(1) p_x orbitals participate in the band formation, while O(1') p_y suffers from cancellation of the left and right overlaps. The weak O(1)-O(1') overlaps also cancel out, as shown in the figure.

conjunction with the piezoelectric-driven *in-situ* strain is particularly *challenging*, because of the severe constraint on sample size, for which particular attention was paid to enhance the signal-to-noise ratio for all these measurements.

III. RESULTS AND DISCUSSION

The geometry of our experiment is depicted in Fig. 1(a) [33]. Each Ru ion is coordinated octahedrally by four planar O(1) and two apical O(2) oxygen sites, with a small elongation along the \mathbf{c} -axis. While \mathbf{a} -axis strain ε_{aa} renders the sites O(1) and O(1') crystallographically inequivalent, their local symmetries are different even for the unstrained case in the case of the external field $\mathbf{B} \parallel \mathbf{b}$. The field-sweep spectra in Fig. S2 are described by parameters (shifts, electric field gradient (EFG)) similar to previous reports for ^{17}O NMR in the unstrained Sr_2RuO_4 [28, 33], with five NMR transitions for each of 3(2) dis-

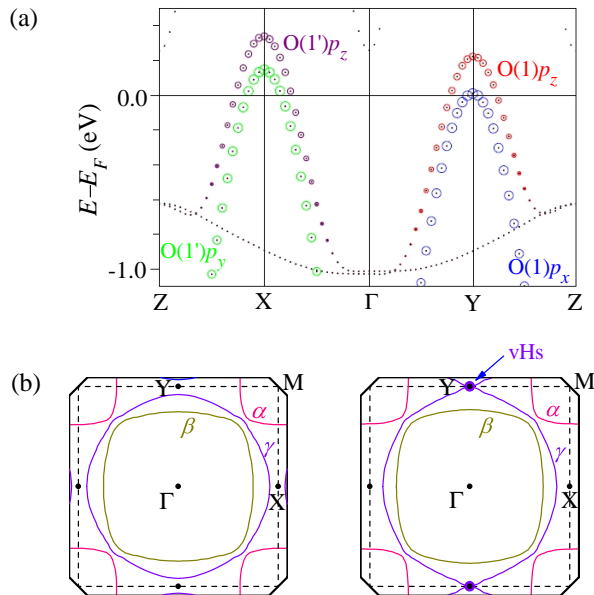


FIG. 2. (a) Bands along the Γ -X and Γ -Y directions. The partial weights of the $O(1)p_x$, $O(1')p_y$, $O(1)p_z$, and $O(1')p_z$ orbitals are shown in green, blue, red and purple, respectively. Other oxygen orbitals have far lesser weight near the Fermi energy. (b) Depictions of the 2D Fermi surfaces, with quasi-2D γ (d_{xy}) and q1D α, β ($d_{zx,yz}$) bands.

tinct sites for $\mathbf{B} \parallel \mathbf{b}$ ($\mathbf{B} \parallel \mathbf{c}$) [31].

The most relevant orbitals for the ^{17}O couplings are Ru $4d$ t_{2g} , which hybridizes with O p states to form the quasi-2D γ band, predominantly from the d_{xy} orbital, and similarly the quasi-1D α and β bands from the $d_{zx,yz}$ orbitals, Fig. 1b. The spin-orbit coupling (SOC) mixes these. While mixing is strongest along the Brillouin Zone diagonal (Γ -M in momentum space, see Fig. 2b) [34, 35], it is more important here that it mixes the d_{xy} and d_{yz} bands at Y. The latter has the effect of pushing down the lower band (d_{xy}) by about 20 meV, which shifts the critical strain ε_v where the Lifshitz transition shows up in the calculations, from about $\sim -1.0\%$ to $\sim -0.65\%$. Additional mass renormalization, not accounted for in the density functional calculations, reduces the critical strain still further, consistent with the experimentally observed maximum in T_c between -0.55% and -0.60% [25, 31].

The ^{17}O NMR absorption spectra under varying strain conditions are shown in Fig. 3. The two panels include absorption spectra covering the central transition for the three sites O(1), O(1'), O(2), measured with carrier frequency $f_0 = 46.80$ MHz and magnetic field $B=8.0970$ T, applied parallel to \mathbf{b} (left panel) and \mathbf{c} axes (right panel), respectively. The peaks for O(1), O(1'), O(2) appear at the labelled frequencies, measured relative to f_0 . The vertical dashed lines correspond to zero shift. O(2), having relatively minor contribution to the Ru bands (there

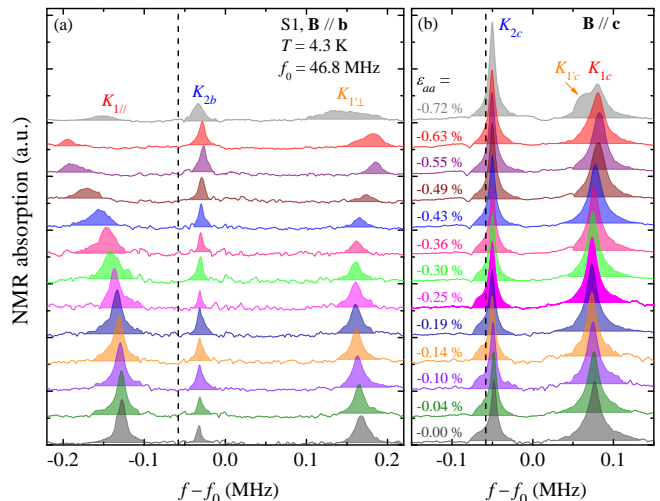


FIG. 3. Absorption spectra of the central transitions ($\frac{1}{2} \leftrightarrow -\frac{1}{2}$) of O(1), O(1') and O(2) at various strains for magnetic field along \mathbf{b} - (left), \mathbf{c} -axes (right). The measurements were carried out at fixed temperature ($T=4.3$ K) and field ($B=8.0970$ T) and radio frequency $f_0=46.80$ MHz. The curves are vertically offset for clarity. The dash vertical line corresponds to $^{17}\gamma=-5.7719$ MHz/T (D_2^{17}O) [29] with zero shift.

is only a weak coupling of the O(2) $p_{x,y}$ with Ru $d_{zx,yz}$ orbitals, respectively) exhibits a very small Knight shift. In contrast, Knight shifts for O(1) and O(1') vary strongly and show clear extrema where the putative vHs appears, at ε_v , defined as where $T_c(\varepsilon_{aa})$ is largest. The anomaly is most pronounced for the in-plane field orientation. For larger strains, there is significant broadening, which could result from a strong strain dependence of the spin susceptibility combined with a distribution of strains within the sample. In the right-hand panel, O(1,1') absorption peaks appear indistinguishable at small strain, with pronounced broadening and splitting appearing for strains exceeding ε_v . The NMR shifts K , defined as the percentage of the shift of resonance frequency with respect to that in D_2^{17}O , are shown as a function of ε_{aa} in Fig. 4.

In metals, the NMR shift is governed by three main contributions to the local field (in addition to the applied field): (i) isotropic coupling from the Fermi contact interaction and core polarization, (ii) anisotropic coupling of the dipolar field generated by the electronic spin away from the nucleus, and (iii) fields generated by orbital currents. This partitioning of the hyperfine field contributions can be summarized as

$$\mathbf{h}(\mathbf{r}) = \mathbf{h}_s + \mathbf{h}_d + \mathbf{h}_o = -\beta \left[\frac{8\pi s \delta(\mathbf{r})}{3} + \frac{3\mathbf{r}(\mathbf{r} \cdot \mathbf{s}) - r^2 \mathbf{s}}{r^5} + \frac{\mathbf{L}}{r^3} \right], \quad (1)$$

where \mathbf{s} is the spin moment of an electron, and \mathbf{L} its orbital moment. Note that \mathbf{h}_s has no anisotropy, while \mathbf{h}_d gives no isotropic contribution (\mathbf{h}_o has both).

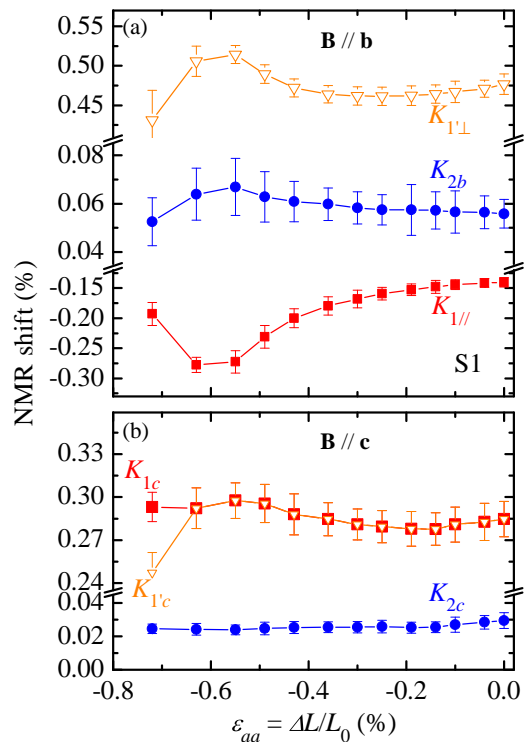


FIG. 4. Measured NMR shifts for $\mathbf{B} \parallel \mathbf{b}$ (a) and for $\mathbf{B} \parallel \mathbf{c}$ (b).

The net spin magnetization is written as

$$M = \chi H_0 \quad (2)$$

where the full uniform susceptibility χ can be approximately written in an RPA-type way [36] using the Stoner factor S :

$$\chi = \chi_0 / [1 - IN(E_F)] \quad (3)$$

$$= S\chi_0, \quad (4)$$

where χ_0 is the *noninteracting* susceptibility equal to (neglecting spin-orbit effects) the density of states. The total uniform magnetic field is the sum of the external and the screening field, the latter being enhanced compared to the noninteracting case by the factor S . Note that the orbital moment \mathbf{L} in Eq. (1) is assumed to be generated by the spin magnetization through spin-orbit coupling; in addition, there is another orbital term (paramagnetic van Vleck), which is not enhanced in the same way as χ .

As discussed in some detail below, S can be more sensitive to the enhancement of the DOS than χ_0 itself, and further is important as a mechanism for transferring anomalous responses to orbitals other than Ru d_{xy}

and the corresponding hybridizing Op orbitals. The experimentally measured χ is enhanced by about a factor of 7 compared to the DFT DOS [23], originating with both mass renormalization ($m^*/m_0 \sim 3.5$ [3]), and Stoner factor ($S \sim 2$). Using Eq. (4) one can then estimate $IN(E_F) \approx 0.5$. Note that the calculated DOS (Fig. 5) is enhanced by about 30% at the vHs. If m^*/m_0 and I are strain independent, the maximal S (at the vHs) is $S_{\max} \sim 3$ and $\chi/\chi_0 \sim 10$, which compare favorably to the shift measurements plotted in Fig. 4. Deviations from standard Fermi Liquid behavior, as reported in relation to recent transport experiments [26] may be connected to the enhanced Stoner factor near the critical strain. Observed is a crossover temperature T^* , above which the derivative $\delta = d(\log \Delta\rho)/d(\log T)$ changes from the Fermi-liquid result $\delta = 2$ to a value ~ 1.5 - 1.6 . This is close to what is expected for ferromagnetic spin-fluctuation behavior ($\delta \sim 4/3$ - $5/3$) [37]. T^* varies strongly with strain (see Fig. S1b [31]), and further, is minimized at ϵ_p . The interpretation of Ref. [26] reasonably associates the behavior with proximity to the vHs [38]; however, both the singular DOS and enhanced S may play a role.

For insight into the strain-induced changes, and particularly those associated with the vHs, Density Functional calculations using the Linear Augmented Plane Wave package WIEN2k [39] were performed, including spin-orbit interaction. The specific objective was to extract at least semi-quantitative information about the origin, evolution, and relative importance of the individual contributions in Eq. (1) to the net Knight shifts. A local density approximation (LDA) for the exchange-correlation functional, a k -point mesh of $41 \times 41 \times 41$, and the expansion parameter $RK_{\max}=7$ were utilized. Further, the optimized structures of Ref. [25] were used, and then interpolated to assure that the strain at which the vHs crosses the Fermi level is included. It turns out that the proximity to a quantum critical point forced some adjustments to the standard procedure. A means for Knight shift evaluation within DFT is to apply an external magnetic field H_0 , then compute the generated hyperfine fields. DFT overestimates the tendency to magnetism, because in reality the Hund's rule derived interaction I and, correspondingly, the Stoner renormalization S are reduced by quantum fluctuations that are not accounted for in a mean-field approach. In addition, the calculated peak in DOS is very narrow, with full width at half (the calculated) maximum of ~ 3 meV, and holds only $0.0015 e^-$ in each spin channel. As a result, an external field producing sufficiently strong hyperfine fields (compared to the computational noise), is too large to properly monitor the vHs peak. Still, the calculations at larger fields produce useful information about the origin of the net Knight shifts in terms of individual contributions in Eq. (1).

The magnetic instability was avoided in two ways: (1) the less magnetic LDA was utilized, rather than the GGA

functional, and (2) an *ad hoc* scaling factor was applied, which effectively reduced the Hund's coupling, somewhat arbitrarily, by a factor of two [40]. This comes at some cost, however. While it allows monitoring of the changes with strain, the overall scale of the calculated Knight shifts is not very accurate. Also, the LDA functional is less accurate than GGA in term of addressing the structural effects, and therefore the critical strain at which the vHs crosses the Fermi level is overestimated by about 50%. Therefore, all computational results below are presented as a function of the reduced strain, $\varepsilon_{aa}/\varepsilon_v$. Note that important by-products of these calculations are the full uniform susceptibility $\chi = M/H$, where M is the total magnetization induced by the field H , and the one-electron susceptibility $\chi_0 = \mu_B^2 N(E_F)$, and therefore also the ratio, $S = \chi/\chi_0$.

The resulting partial densities of states and character-projected bands in Sr_2RuO_4 are shown in Figs. 5 and 2(a). Only $\text{O}(1)p_x$ states are sensitive to the vHs, as expected from symmetry considerations (Fig. 1b). Indeed, at Y, only $\text{O}(1)p_x$ orbitals couple by symmetry with $\text{Ru}d_{xy}$ states, and then, one might infer that only the $\text{O}(1)$ Knight shift should be affected by the DOS peak at the vHs. This is borne out by the DOS calculations. However, on general grounds, all sites are sensitive through the Stoner enhancement S . Indeed, all measured Knight shifts are affected by strain (Fig. 4), with $K_{1\parallel}$ more so, presumably because of the direct influence of increased γ DOS. The last point is also important because it associates the enhanced DOS and S at the critical strain, with the vHs at Y, where the $\text{O}(1)p_x$ orbital is the only O orbital with considerable weight. Further evidence for the narrow vHs and its influence is shown in Fig. 6, which depicts shifts with strikingly strong field and temperature dependences. The observations are qualitatively consistent with comparable energy scales for Zeeman, thermal, and vHs terms, where, for instance, the broadening of the Fermi distribution progressively weakens the sensitivity of thermodynamic properties to the vHs, even when it is situated precisely at the chemical potential [41]. Similar observations for the magnetization were previously reported in a doping study, in which the effects of substitution of La for Sr in $\text{Sr}_{2-y}\text{La}_y\text{RuO}_4$ were interpreted as evidence for moving γ -band Fermi energy to the X and Y points of the Brillouin Zone [42].

For a semiquantitative evaluation of the Stoner enhancement and impact on the observable quantities, the data were contrasted to the results of the DFT calculations. As discussed in the previous section, the inherent deficiency of the DFT calculations for such a strongly correlated material as Sr_2RuO_4 forced deviations from the usual routine. The standard calculations, as used, for instance, in Ref. [25], are unstable against spontaneous formation of a ferromagnetic state. The tendency toward this instability was reduced, somewhat arbitrar-

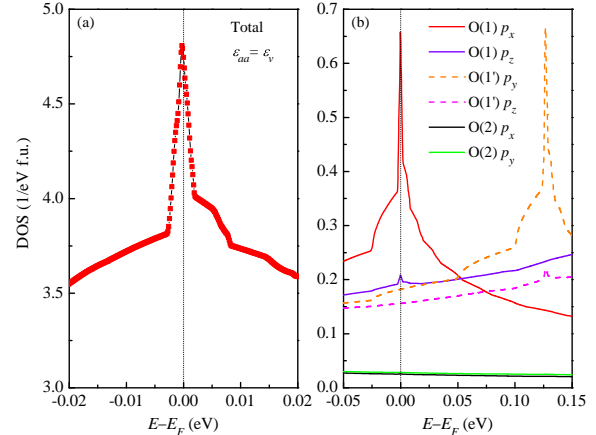


FIG. 5. (a) Calculated density of states (DOS) at the critical strain, at which the calculated van Hove singularity is located exactly at the Fermi level. Note the very small width (3 meV) and weight (0.0015 e^- per spin channel) of the peak in DOS. (b) Partial DOS projected onto different O orbitals. The orbitals that are not shown have negligible weight.

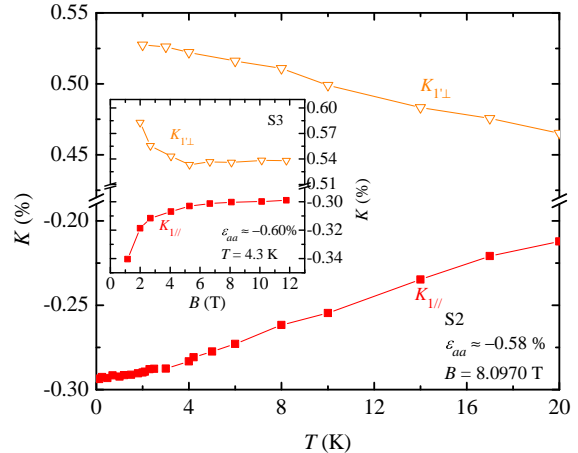


FIG. 6. Main panel, temperature dependence of $K_{1\parallel}$ and $K_{1'\perp}$, evaluated at the critical strain ε_v , $B = 8.0970$ T, and $\mathbf{B} \parallel \mathbf{b}$. Inset, field dependence of $K_{1\parallel}$ and $K_{1'\perp}$ measured at ε_v and 4.3 K.

ily, by scaling the Hund's coupling by half. This ensured numerically stable calculations in external fields up to at least 5 T, even at $\varepsilon_{aa} = \varepsilon_v$. The impact of the reduced Hund's coupling appears to produce systematic errors in related absolute parameters, but less so for the relative changes induced by strain. For example, for the selected scaling, Fig. 7 indicates that the calculated $\chi(\varepsilon_{aa} = 0)$ renormalization is $\sim 60\%$, whereas the known

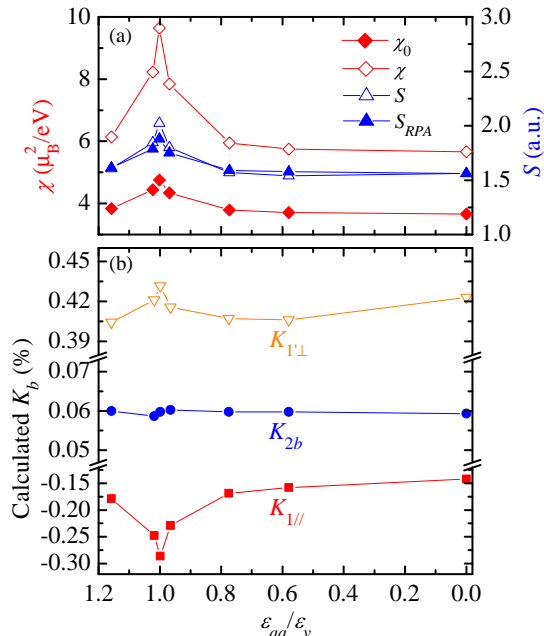


FIG. 7. (a) Calculated magnetic susceptibility. $\chi_0 \equiv \mu_B^2 N(E_F)$ is the noninteracting susceptibility, χ is obtained by dividing the calculated magnetization by the applied field, $M/\mu_B H$. The full Stoner factor $S = \chi/\chi_0$, and $S_{RPA} = 1/(1 - I\chi_0)$, where $I = 0.2$ eV. (b) Calculated total Knight shifts for $\mathbf{H} \parallel \mathbf{b}$ for the three sites, O(1), O(1') and O(2), as a function of normalized strain. See the text for details.

correlation-induced mass enhancement is 3.5 [3]. Therefore, the downscaling is too strong. Given this caveat, at the critical strain, χ is enhanced over $\chi(0)$ by about 70%, while $S(\varepsilon_v)$ is about 30% larger than $S(0)$. Thus, expected enhancements are ~ 1.3 for $K_{1'\perp}$ and K_{2b} , and ~ 1.7 for $K_{1\parallel}$, all consistent with the calculated shown in Fig. 7b.

Relatively strain-independent orbital terms were calculated for the shifts of all three sites, as would occur for a van Vleck-dominated response. Since this is notoriously difficult to calculate in DFT, these orbital contributions were adjusted to ensure a good agreement with the experiment. The constants were, respectively, -0.07% , 0.35% and 0.06% for $K_{1\parallel}$, $K_{1'\perp}$ and K_{2b} . We emphasize that the described procedure is too approximate to assign particular importance to the exact numbers; however the resulting, indeed rather good agreement between the calculated and measured hyperfine contributions, lends some validity to the approach and interpretation.

Therefore, the qualitative conclusions are as follows: (1) there are two mechanisms for enhancing the Knight shifts near the critical strain, one applicable to all sites and field directions, and the other only to $K_{1\parallel}$. Both

are directly related to the DOS enhancement and show unambiguously that the maximum in T_c indeed coincides with that in DOS; (2) ferromagnetic spin fluctuations intensify substantially at the same strain, and may play a key role in boosting T_c . Furthermore, it provides a natural explanation to the recent resistivity measurements on strained samples.

Some comments on the data collected for field aligned parallel the \mathbf{c} -axis are in order. In principle, one would expect similar behavior to that for the in-plane field, however, it appears that K_c behaves in a way difficult to rationalize in total. For strain $\varepsilon_{aa} \leq -0.63\%$, a single absorption peak at $\sim 0.28\%$ shift is observed for O(1,1'), with only a small increase in the range of ε_v . For larger strain, $\varepsilon_{aa} = -0.72\%$, the peak broadens considerably, and could be construed as exhibiting two components, but with drastically reduced first moment. The drop in intensity is likely a T_1 effect, a consequence of a too rapid pulse repetition rate (see Fig. S5, SM). The apparent “splitting” and distorted lineshape are consistent with what could result from a strain gradient along with a nonlinear variation of shift with strain. The main challenge, however, is to explain the observed evolution on approaching ε_v from smaller strain, where the DFT calculations indicate larger shifts for O(1) than for O(1').

It is possible that the orbital contributions play an important role in this case. Interestingly, for the orbital part of K_{1c} , and to some extent, of $K_{1'c}$, the calculations predict a sizeable enhancement, suggesting that the van Vleck contribution is not dominant, or, at least, less prominent here than for the in-plane fields, and, conversely, the SOC induces sizeable orbital Knight shifts. Moreover, the sign of this orbital contribution is opposite to the spin shifts, so there is a tendency toward cancellation. It is believed that correlation effects enhance the SOC in Sr_2RuO_4 by about a factor of two [43]. Empirically, if the O(1) and O(1') shifts are assumed to be entirely generated by SOC, while the O(2) shift is entirely van Vleck, a reasonable agreement with experiment is obtained, but with small but not negligible peak splittings for strains near ε_v (Fig. S6). Clearly, the NMR spectra for the field parallel to \mathbf{c} require further investigation.

IV. FURTHER CONSIDERATIONS REGARDING STONER RENORMALIZATION

The experiments and calculations clearly demonstrate the importance of Stoner renormalization near the critical strain, but this is evaluated only semiquantitatively. For example, the RPA-like Eq. (4) implies a uniform renormalization of the exchange splitting over the entire Fermi surface, whereas the calculations allow for comparison of the induced magnetization $M(H)$ to the Pauli formula, $M_0(H) = \mu_B^2 N(E_F)H$. Dividing the calculated $M(H)$ by H we can compute the full DFT susceptibility,

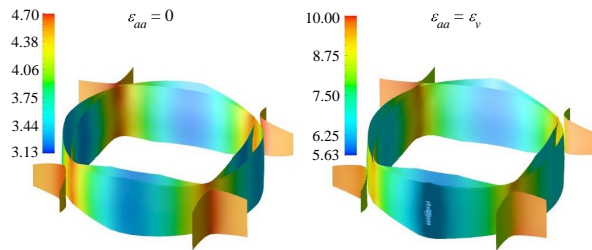


FIG. 8. Calculated Fermi surfaces with no orthorhombic strain (left) and the strain corresponding to the vHs (right). The surfaces are colored with the Stoner factor S (nonrelativistic). Note the different color scales for the two panels.

and dividing M by M_0 the Stoner factor S . The result is shown in Fig. 7. The RPA Eq. (4) works reasonably well, provided the Stoner exchange parameter I as an adjustable parameter. However, this agreement may be somewhat misleading, since S varies substantially over the Fermi surface (depicted in Fig. 8). Note also that S , for the same external field, is most strongly enhanced for the α and β bands, and less so for the γ band, and that this enhancement is indeed about twice as strong at the critical strain than for the unstrained structure. Overall, in the former the Stoner factor S varies between 3.2 and 4.7, and in the latter between 5.7 and 10.0, about a factor of two larger than for the unstrained structure. Consequently, it is entirely possible that this variation will weight differently the dipole and the spin-contact contributions. This is consistent with the fact that the temperature dependence of the in-plane, and only in-plane Knight shifts is opposite to that of the uniform susceptibility at $T \lesssim 100$ K, and only these are affected by the vHs in our experiment[28].

Given the proximity to magnetism, it is natural to assume that spin fluctuations play a major role in transport scattering. Moriya *et al* worked out a theory of paramagnon scattering in the uniform Stoner approximation[37], but as shown here, it is not accurate for Sr_2RuO_4 . Moreover, Sr_2RuO_4 combines both anti-ferromagnetic (not enhanced by the vHs) and ferromagnetic (enhanced) fluctuations. In favor of the applicability of Moriya's theory to Sr_2RuO_4 is that the full susceptibility as evaluated from neutron scattering results [23] and interpreted in the framework of Moriya's theory, generates mass renormalization in agreement with specific heat data. Within the same framework, the resistivity is expected to change from the usual (Fermi Liquid) low-temperature T -quadratic behavior to $\approx T^{1.6}$ at a crossover temperature $T^* \propto S^{-1}$. The transport measurements in Ref. [26] revealed such behavior, where

moreover, the crossover temperature T^* exhibits a pronounced minimum near ε_v (Fig. S1b in SM). This is fully consistent with the present conclusion that S peaks at the same strain.

V. CONCLUSION

It is demonstrated, by means of the NMR spectroscopy under uniaxial stress, and corresponding density functional calculations, that there are *two* different effects associated with the strain-induced vHs, which both need to be taken into account, namely the enhancement of the DOS associated with the γ -band Fermi energy passing through the vHs at the Y point of the Brillouin Zone, and a substantial Stoner enhancement S . This finding has immediate ramifications for superconductivity. Namely, first, the DOS is enhanced near the vHs point. In the first approximation, this effect strongly favors some singlet pairings, such as extended s , $d_{zx} \pm id_{yz}$ or $d_{x^2-y^2}$, mildly favors the d_{xy} pairing, and less so any triplet pairing. However, this enhancement of the DOS, through the Stoner factor, boosts FM spin fluctuations, which favors a triplet states and would seem to *disfavor* singlet pairing. Experimentally and theoretically, these two effects are comparable, and therefore it is unclear which is stronger. More information will be gained by studying NMR in the superconducting state as a function of strain; measurements are currently underway.

ACKNOWLEDGMENTS

We thank S. A. Kivelson, S. Raghu, J. D. Thompson, and F. Zhang for insightful discussions, and J. D. Thompson for magnetic properties characterization. Work at Los Alamos was funded by Laboratory Directed Research and Development (LDRD) program, and Y.L. acknowledges partial support through the LDRD and 1000 Youth Talents Plan of China. N.K. acknowledges the support from JSPS KAKNHI (18K04715). I.I.M was supported by ONR through the NRL basic research program. This work was supported in part by the National Science Foundation (DMR-1410343 and DMR-1709304).

* mpzslyk@gmail.com

† brown@physics.ucla.edu

- [1] Y. Maeno, H. Hashimoto, K. Yoshida, S. Nishizaki, T. Fujita, J. G. Bednorz, and F. Lichtenberg, *Superconductivity in a layered perovskite without copper*, *Nature* **372**, 532 (1994).
- [2] T. Rice and M. Sigrist, *Sr_2RuO_4 : an electronic analogue of ^3He ?*, *J. Phys.: Condens. Matter* **7**, L643 (1995).

- [3] A. P. Mackenzie and Y. Maeno, *The superconductivity of Sr_2RuO_4 and the physics of spin-triplet pairing*, *Rev. Mod. Phys.* **75**, 657 (2003).
- [4] Y. Maeno, S. Kittaka, T. Nomura, S. Yonezawa, and K. Ishida, *Evaluation of Spin-Triplet Superconductivity in Sr_2RuO_4* , *J. Phys. Soc. Jpn.* **81**, 011009 (2012).
- [5] C. Kallin, *Chiral p -wave order in Sr_2RuO_4* Rep. Prog. Phys. **75**, 042501 (2012).
- [6] A. P. Mackenzie, T. Scaffidi, C. W. Hicks, and Y. Maeno, *Even odder after twenty-three years: the superconducting order parameter puzzle of Sr_2RuO_4* , *npj Quantum Materials* **2**, 40 (2017).
- [7] G. M. Luke, Y. Fudamoto, K. M. Kojima, M. I. Larkin, J. Merrin, B. Nachumi, Y. J. Uemura, Y. Maeno, Z. Q. Mao, Y. Mori, et al., *Time-reversal symmetry-breaking superconductivity in Sr_2RuO_4* , *Nature* **394**, 558 (1998).
- [8] J. Xia, Y. Maeno, P. T. Beyersdorf, M. M. Fejer, and A. Kapitulnik, *High Resolution Polar Kerr Effect Measurements of Sr_2RuO_4 : Evidence for Broken Time-Reversal Symmetry in the Superconducting State*, *Phys. Rev. Lett.* **97**, 167002 (2006).
- [9] K. Ishida, H. Mukuda, Y. Kitaoka, K. Asayama, Z. Q. Mao, Y. Mori, and Y. Maeno, *Spin-triplet superconductivity in Sr_2RuO_4 identified by ^{17}O Knight shift*, *Nature* **369**, 658 (1998).
- [10] H. Murakawa, K. Ishida, K. Kitagawa, Z. Q. Mao, and Y. Maeno, *Measurement of the ^{101}Ru -Knight Shift of Superconducting Sr_2RuO_4 in a Parallel Magnetic Field*, *Phys. Rev. Lett.* **93**, 167004 (2004).
- [11] J. A. Duffy, S. M. Hayden, Y. Maeno, Z. Mao, J. Kulda, and G. J. McIntyre, *Polarized-Neutron Scattering Study of the Cooper-Pair Moment in Sr_2RuO_4* , *Phys. Rev. Lett.* **85**, 5412 (2000).
- [12] J. R. Kirtley, C. Kallin, C. W. Hicks, E.-A. Kim, Y. Liu, K. A. Moler, Y. Maeno, and K. D. Nelson, *Upper limit on spontaneous supercurrents in Sr_2RuO_4* , *Phys. Rev. B* **76**, 014526 (2007).
- [13] C. W. Hicks, J. R. Kirtley, T. M. Lippman, N. C. Koshnick, M. E. Huber, Y. Maeno, W. M. Yuhasz, M. B. Maple, and K. A. Moler, *Limits on superconductivity-related magnetization Sr_2RuO_4 and $PrOs_4Sb_{12}$ from scanning SQUID microscopy*, *Phys. Rev. B* **81**, 214501 (2010).
- [14] S. Yonezawa, T. Kajikawa, and Y. Maeno, *First-Order Superconducting Transition of Sr_2RuO_4* , *Phys. Rev. Lett.* **110**, 077003 (2013).
- [15] E. Hassinger, P. Bourgeois-Hope, H. Taniguchi, S. R. de Cotret, G. Grissonnanche, M. S. Anwar, Y. Maeno, N. Doiron-Leyraud, and L. Taillefer, *Vertical Line Nodes in the Superconducting Gap Structure of Sr_2RuO_4* , *Phys. Rev. X* **7**, 011032 (2017).
- [16] S. Kittaka, S. Nakamura, T. Sakakibara, N. Kikugawa, T. Terashima, S. Uji, D. A. Sokolov, A. P. Mackenzie, K. Irie, Y. Tsutsumi, et al., *Searching for Gap Zeros in Sr_2RuO_4 via Field-Angle-Dependent Specific-Heat Measurement*, *J. Phys. Soc. Jpn.* **87**, 093703 (2018).
- [17] B. Kim, S. Khmelevskiy, I. I. Mazin, D. F. Agterberg, and C. Franchini, *Anisotropy of magnetic interactions and symmetry of the order parameter in unconventional superconductor Sr_2RuO_4* , *npj Quantum Materials* **2**, 37 (2017).
- [18] I. I. Mazin and D. J. Singh, *Electronic structure and magnetism in Ru-based perovskites*, *Phys. Rev. B* **56**, 2556 (1997).
- [19] L. de' Medici, J. Mravlje, and A. Georges, *Janus-Faced Influence of Hund's Rule Coupling in Strongly Correlated Materials*, *Phys. Rev. Lett.* **107**, 256401 (2011).
- [20] A. Georges, L. de' Medici, and J. Mravlje, *Strong Correlations from Hund's Coupling*, *Annu. Rev. Condens. Matter Phys.* **4**, 137 (2013).
- [21] Y. Sidis, M. Braden, P. Bourges, B. Hennion, S. NishiZaki, Y. Maeno, and Y. Mori, *Evidence for Incommensurate Spin Fluctuations in Sr_2RuO_4* , *Phys. Rev. Lett.* **83**, 3320 (1999).
- [22] I. I. Mazin and D. J. Singh, *Competitions in Layered Ruthenates: Ferromagnetism versus Antiferromagnetism and Triplet versus Singlet Pairing*, *Phys. Rev. Lett.* **82**, 4324 (1999).
- [23] P. Steffens, Y. Sidis, J. Kulda, Z. Q. Mao, Y. Maeno, I. Mazin, and M. Braden, *Spin fluctuations in Sr_2RuO_4 from polarized neutron scattering: implications for superconductivity* arXiv: 1808.05855 (2018).
- [24] A. Damascelli, D. H. Lu, K. M. Shen, N. P. Armitage, F. Ronning, D. L. Feng, C. Kim, Z.-X. Shen, T. Kimura, Y. Tokura, et al., *Fermi Surface, Surface States, and Surface Reconstruction in Sr_2RuO_4* , *Phys. Rev. Lett.* **85**, 5194 (2000).
- [25] A. Steppke, L. Zhao, M. E. Barber, T. Scaffidi, F. Jerzembeck, H. Rosner, A. S. Gibbs, Y. Maeno, S. H. Simon, A. P. Mackenzie, et al., *Strong peak in T_c of Sr_2RuO_4 under uniaxial pressure*, *Science* **355** (2017).
- [26] M. E. Barber, A. S. Gibbs, Y. Maeno, A. P. Mackenzie, and C. W. Hicks, *Resistivity in the Vicinity of a van Hove Singularity: Sr_2RuO_4 under Uniaxial Pressure*, *Phys. Rev. Lett.* **120**, 076602 (2018).
- [27] S. Kivelson, private communication.
- [28] T. Imai, A. W. Hunt, K. R. Thurber, and F. C. Chou, *^{17}O NMR Evidence for Orbital Dependent Ferromagnetic Correlations in Sr_2RuO_4* , *Phys. Rev. Lett.* **81**, 3006 (1998).
- [29] R. K. Harris, E. D. Becker, S. M. C. de Menezes, R. Goodfellow, and P. Granger, *NMR nomenclature. Nuclear spin properties and conventions for chemical shifts (IUPAC Recommendations 2001)*, *Pure and Applied Chemistry* **73**, 1795 (2001).
- [30] A post-anneal in air at reduced temperatures (ca. 450 °C) led to smaller-than-expected absorption from the apical O(2) sites, indicating that the ^{17}O substitution to the O(1) sites likely proceeds through the apical sites.
- [31] Supplementary Material, this article.
- [32] The clamping structure is not perfectly rigid, and as a consequence, the actual sample compression is smaller than what is measured by the dilatometer [44].
- [33] H. Mukuda, K. Ishida, Y. Kitaoka, K. Asayama, Z. Mao, Y. Mori, and Y. Maeno, *Novel Character of Spin Fluctuations in Spin-Triplet Superconductor Sr_2RuO_4 ^{17}O -NMR Study*, *J. Phys. Soc. Jpn.* **67**, 3945 (1998).
- [34] E. Pavarini and I. I. Mazin, *First-principles study of spin-orbit effects and NMR in Sr_2RuO_4* , *Phys. Rev. B* **74**, 035115 (2006).
- [35] M. W. Haverkort, I. S. Elfimov, L. H. Tjeng, G. A. Sawatzky, and A. Damascelli, *Strong Spin-Orbit Coupling Effects on the Fermi Surface of Sr_2RuO_4 and Sr_2RhO_4* , *Phys. Rev. Lett.* **101**, 026406 (2008).
- [36] In principle, the polarization operators and the Stoner factors in this formula are matrices in the band indices and reciprocal lattice vectors. In the discussion here, we neglect these complexities.

- [37] G. R. Stewart, *Non-Fermi-liquid behavior in d- and f-electron metals*, *Rev. Mod. Phys.* **73**, 797 (2001).
- [38] R. Hlubina, *Effect of impurities on the transport properties in the Van Hove scenario*, *Phys. Rev. B* **53**, 11344 (1996).
- [39] P. Blaha, K. Schwarz, G. Madsen, D. Kvasnicka, and J. Luitz, *WIEN2k, An augmented Plane Wave + Local Orbitals Program for Calculating Crystal Properties* (Techn. Universitat Wien, Austria, 2001).
- [40] L. Ortenzi, I. I. Mazin, P. Blaha, and L. Boeri, *Accounting for spin fluctuations beyond local spin density approximation in the density functional theory*, *Phys. Rev. B* **86**, 064437 (2012).
- [41] R. Nourafkan and S. Acheche, *Temperature dependence of NMR Knight shift in pnictides: proximity to a van Hove singularity* arXiv: 1807.09683 (2018).
- [42] N. Kikugawa, C. Bergemann, A. P. Mackenzie, and Y. Maeno, *Band-selective modification of the magnetic fluctuations in Sr_2RuO_4 : A study of substitution effects*, *Phys. Rev. B* **70**, 134520 (2004).
- [43] M. Kim, J. Mravlje, M. Ferrero, O. Parcollet, and A. Georges, *Spin-Orbit Coupling and Electronic Correlations in Sr_2RuO_4* , *Phys. Rev. Lett.* **120**, 126401 (2018).
- [44] C. W. Hicks, M. E. Barber, S. D. Edkins, D. O. Brodsky, and A. P. Mackenzie, *Piezoelectric-based apparatus for strain tuning*, *Rev. Sci. Instrum.* **85**, 065003 (2014).
- [45] C. W. Hicks, D. O. Brodsky, E. A. Yelland, A. S. Gibbs, J. A. N. Bruin, M. E. Barber, S. D. Edkins, K. Nishimura, S. Yonezawa, Y. Maeno, et al., *Strong Increase of T_c of Sr_2RuO_4 Under Both Tensile and Compressive Strain*, *Science* **344**, 283 (2014).
- [46] The capacitive reading is an upper bound. In practice, the elasticity of the mounting structure, including the epoxy, leads to reductions. In this article, we have assumed a corrective factor of 0.8, following Ref. [25]. Independent assessment will be evaluated in future benchmark studies.
- [47] K. Deguchi, Z. Q. Mao, and Y. Maeno, *Determination of the Superconducting Gap Structure in All Bands of the Spin-Triplet Superconductor Sr_2RuO_4* , *J. Phys. Soc. Jpn.* **73**, 1313 (2004).
- [48] N. Okuda, T. Suzuki, Z. Mao, Y. Maeno, and T. Fujita, *Unconventional Strain Dependence of Superconductivity in Spin-Triplet Superconductor Sr_2RuO_4* , *J. Phys. Soc. Jpn.* **71**, 1134 (2002).
- [49] M. E. Garcia and K. H. Bennemann, *Theoretical study of the structural dependence of nuclear quadrupole frequencies in high- T_c superconductors*, *Phys. Rev. B* **40**, 8809 (1989).
- [50] T. Oguchi, *Electronic band structure of the superconductor Sr_2RuO_4* , *Phys. Rev. B* **51**, 1385 (1995).
- [51] J. Haase, O. P. Sushkov, P. Horsch, and G. V. M. Williams, *Planar Cu and O hole densities in high- T_c cuprates determined with NMR*, *Phys. Rev. B* **69**, 094504 (2004).

Supplemental Material:
Normal state ^{17}O NMR studies of Sr_2RuO_4 under uniaxial stress

Yongkang Luo^{1,7*}, P. Guzman¹, A. P. Dioguardi², A. Pustogow¹, S. M. Thomas², F. Ronning², N. Kikugawa³, D. Sokolov⁴, F. Jerzembeck⁴, A. P. Mackenzie^{4,5}, C. W. Hicks⁴, E. D. Bauer², I. I. Mazin⁶, and S. E. Brown^{1†}
¹*Department of Physics and Astronomy, University of California, Los Angeles, CA 90095, USA;*
²*Los Alamos National Laboratory, Los Alamos, New Mexico 87545, USA;*
³*National Institute for Materials Science, Tsukuba 305-0003, Japan;*
⁴*Max Planck Institute for Chemical Physics of Solids, Dresden 01187, Germany;*
⁵*Scottish Universities Physics Alliance, School of Physics and Astronomy, University of St Andrews, North Haugh, St Andrews KY16 9SS, UK;*
⁶*Code 6393, Naval Research Laboratory, Washington, DC 20375, USA; and*
⁷*Wuhan National High Magnetic Field Center and School of Physics, Huazhong University of Science and Technology, Wuhan 430074, China.*

In this **Supplemental Material (SM)**, we provide the experimental setup, sample characterization, field-swept spectra, spin-lattice relaxation rate and electric field gradient (EFG) results of Sr_2RuO_4 under uniaxial stress, as well as additional theoretical details that further support the discussions in the main text.

SM I: Sample characterizations

Figure S1a is a photograph of the set-up for our NMR measurements under strain. The compressive uniaxial pressure is generated by a set of piezoelectric actuators[45]. A Sr_2RuO_4 sample is glued between two pairs of titanium plates with stycast 2850 (black). To get a perfect filling factor, a small NMR coil (about 25 turns) is made *in-situ* surrounding the sample after the stycast hardens with 25 μm Cu wire.

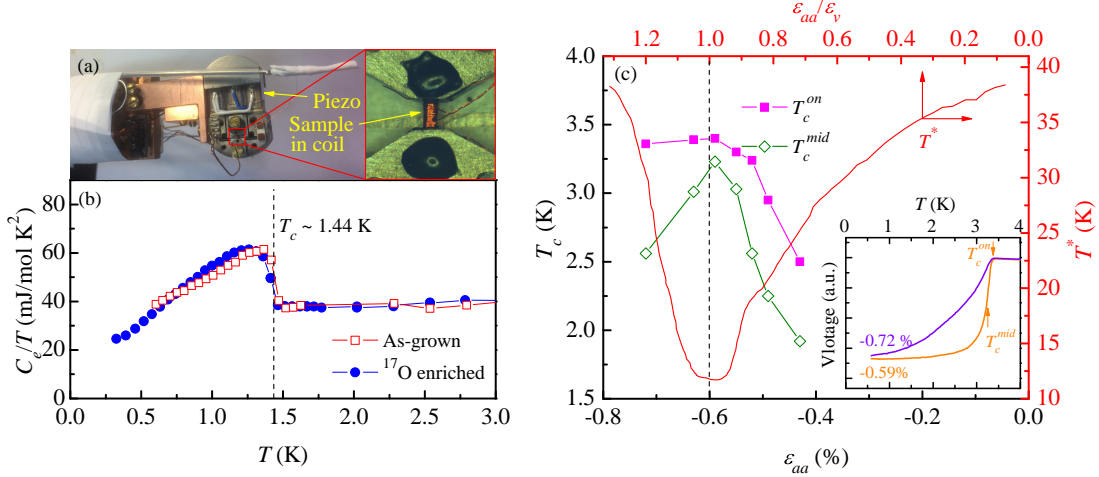


FIG. S1. (a) A photograph of the uniaxial stress apparatus. The stress/strain effect is applied through a set of piezoelectric actuators. The forces are applied uniaxially, and the strain response is measured using a capacitive dilatometer. A small coil is made *in-situ* surrounding the sample that is bonded between two pairs of titanium plates. (b) Electronic specific heat divided by temperature of the sample before and after ^{17}O enrichment. Superconducting transitions are clearly visible at about 1.44 K. (c) Strain dependence of superconducting transition from ac magnetization measurements, with critical temperatures T_c^{on} and T_c^{mid} defined in the inset. Maximal T_c is realized near the strain $\epsilon_{aa} = -0.6\%$. The top-right frame displays the profile of T^* reproduced from Ref. [26]. The strains from the respective experiments are aligned using the respective measured maxima in superconducting critical temperature, $T_c(\epsilon_{aa})$ [46].

The quality of the sample measured is characterized by specific heat measurements, as shown in Fig. S1b. The superconducting transitions are clearly visible in C_e/T before and after annealing in ^{17}O atmosphere, with $T_c \approx 1.44$ K essentially unaffected. Here C_e is the electron contribution to specific heat. The jump in C_e/T at the transition

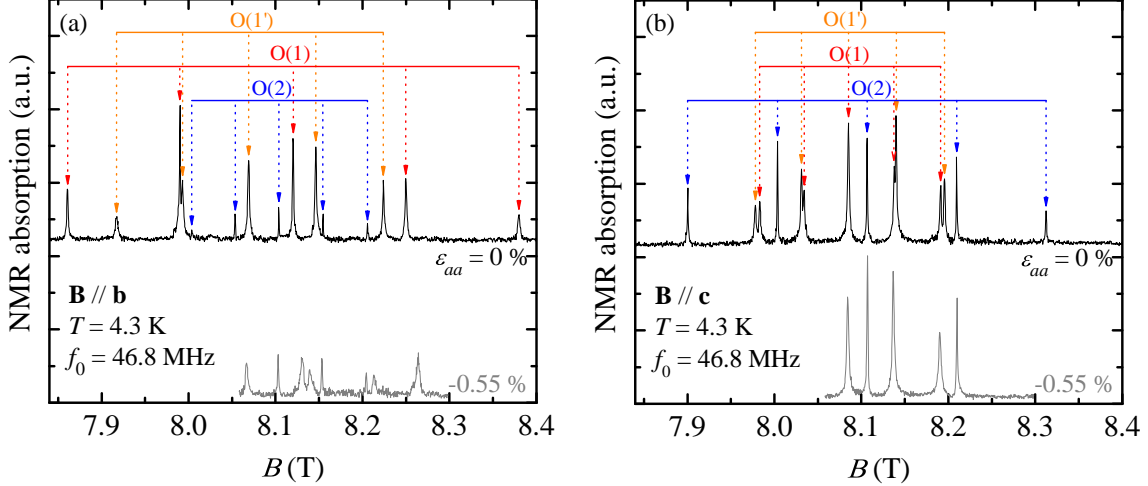


FIG. S2. Comparison of ^{17}O NMR spectra for strain $\varepsilon_{aa}=0$ (black) and -0.55% (grey) where T_c approaches the maximum. (a) measurements with $\mathbf{B} \parallel \mathbf{b}$, and (b) with $\mathbf{B} \parallel \mathbf{c}$. At $\varepsilon_{aa}=0$ and $\mathbf{B} \parallel \mathbf{c}$, the splitting of O(1) and O(1') satellite peaks is due to a small angular misalignment ($\sim 5^\circ$).

as well as the normal state Sommerfeld coefficient are also in good agreement with previous findings[47]. All these guarantee the high quality of the sample studied in this work.

In Fig. S2, we present the field-sweep ^{17}O NMR spectra of Sr_2RuO_4 for both $\mathbf{B} \parallel \mathbf{b}$ (left panel) and $\mathbf{B} \parallel \mathbf{c}$ (right panel). All the peaks in this field region can be assigned to signals from O(1), O(1') and O(2) sites, and no extra peaks can be identified. This excludes the impurity phases from other members in $\text{Sr}_{n+1}\text{Ru}_n\text{O}_{3n+1}$ family. For each O site, it shows one central peak ($\frac{1}{2} \leftrightarrow -\frac{1}{2}$) and four satellite peaks corresponding to $\pm\frac{1}{2} \leftrightarrow \pm\frac{3}{2}$ and $\pm\frac{3}{2} \leftrightarrow \pm\frac{5}{2}$, respectively.

TABLE S1. Comparison of Knight shifts and components of the EFG tensor in Sr_2RuO_4 for $\varepsilon_{aa}=0$ ($T_c=1.44$ K) and -0.55% ($T_c=3.3$ K). Measurements made at 4.3 K. The asymmetry parameter can be calculated by $\eta=(\nu_x-\nu_y)/\nu_z$.

Sites		Quantities	$\varepsilon_{aa}=0$	$\varepsilon_{aa}=-0.55\%$	Note
O(1)	K_1	$K_{1\parallel}$ (%)	-0.15(1)	-0.28(2)	
		K_{1c} (%)	+0.29(1)	+0.30(1)	
	EFG(1)	ν_{1a} (MHz)	-0.444(4)	-0.469(7)	ν_{1y}
		ν_{1b} (MHz)	+0.755(5)	+0.778(9)	$\nu_{1z}=\nu_{1Q}$
		ν_{1c} (MHz)	-0.311(3)	-0.309(5)	ν_{1x}
Asymmetry	η_1	0.175(3)	0.206(5)		
O(1')	$K_{1'}$	$K_{1'\perp}$ (%)	+0.48(1)	+0.52(2)	
		$K_{1'c}$ (%)	+0.29(1)	+0.30(1)	
	EFG(1')	$\nu_{1'a}$ (MHz)	+0.759(6)	+0.730(9)	$\nu_{1'z}=\nu_{1'Q}$
		$\nu_{1'b}$ (MHz)	-0.445(4)	-0.425(6)	$\nu_{1'y}$
		$\nu_{1'c}$ (MHz)	-0.314(4)	-0.305(5)	$\nu_{1'x}$
Asymmetry	$\eta_{1'}$	0.172(3)	0.164(5)		
O(2)	K_2	K_{2b} (%)	+0.055(6)	+0.066(9)	
		K_{2c} (%)	+0.021(5)	+0.015(3)	
	EFG(2)	ν_{2a} (MHz)	-0.300(2)	-0.303(3)	ν_{2y}
		ν_{2b} (MHz)	-0.300(2)	-0.299(3)	ν_{2x}
		ν_{2c} (MHz)	+0.600(3)	+0.602(4)	$\nu_{2z}=\nu_{2Q}$
Asymmetry	η_2	0.000(1)	0.007(2)		

These satellite peaks arise from nuclear quadrupole interaction with the electric field gradient (EFG) at the nuclear

site, as described by

$$H_Q = \frac{eQV_{zz}}{4I(2I-1)}[3\hat{I}_z^2 - \hat{\mathbf{I}}^2 + \eta(\hat{I}_x^2 - \hat{I}_y^2)], \quad (\text{S1})$$

where $\hat{\mathbf{I}}=(\hat{I}_x, \hat{I}_y, \hat{I}_z)$ is nuclear spin operator, Q is nuclear quadrupole moment, and $\eta=(V_{xx}-V_{yy})/V_{zz}$ is the asymmetry parameter with V_{xx} , V_{yy} and V_{zz} being the components of the EFG tensor. Here we adopt the convention $V_{zz} \geq V_{xx} \geq V_{yy}$, and $V_{xx}+V_{yy}+V_{zz}=0$. In Sr_2RuO_4 , V_{zz} is along Ru-O bonding[33]. This allows us to determine principle-axis nuclear quadrupole resonance (NQR) frequency $\nu_Q=\nu_z$ from the spectra shown in Fig. S2. Note that ν_z is related to V_{zz} by

$$\nu_z = \frac{3eQV_{zz}}{2I(I-1)\hbar}. \quad (\text{S2})$$

Other components of NQR frequencies conform to the formula:

$$\nu'_Q = \nu_Q \left[\frac{3 \cos^2 \theta - 1}{2} + \frac{\eta}{2} \sin^2 \theta \cos 2\phi \right], \quad (\text{S3})$$

where θ and ϕ are respectively polar and azimuthal angles as defined in regular \mathbf{xyz} -frames, see Fig. S3a. Eq. (S3) also enables us to verify the sample orientation with respect to magnetic field. In fact, for $\mathbf{B}||\mathbf{c}$ and $\varepsilon_{aa}=0$, we should expect the NQR peaks of O(1) and O(1') to merge. The splitting of them seen in Fig. S2b is a consequence of small angular misalignment which we estimate to be $\theta \sim 5^\circ$ according to Eq. (S3).

Table S1 summarizes all the physical parameters of O(1), O(1') and O(2) sites after the correction of angular misalignment. The results at ambient pressure are in good agreement with that reported by Mukuda *et al* [33].

SM II: Strain dependent ν_Q – experimental and theoretical

Under strain, the peaks of O(2) sites remain essentially unchanged, while both O(1) and O(1') change drastically. In particular, for $\mathbf{B}||\mathbf{c}$, the satellite peaks of O(1) and O(1') merge “coincidentally” when $\varepsilon_{aa}=-0.55\%$, implying that the two move at different rates under strain. The strain dependencies of ν_Q and η are displayed in Fig. S3b-c. Evidently, the changes of ν_Q in O(1) and O(1') are of opposite signs. This is because an expansive strain is induced along \mathbf{b} -axis, *i.e.* $\varepsilon_{bb}>0$, which is characterized by the Poisson’s ratio $-\varepsilon_{bb}/\varepsilon_{aa}=0.40$ for Sr_2RuO_4 [48]. We should note that the ratio of the slopes in $\nu_{1Q}(\varepsilon_{aa})$ and $\nu_{1'Q}(\varepsilon_{aa})$ is very close to Poisson’s ratio.

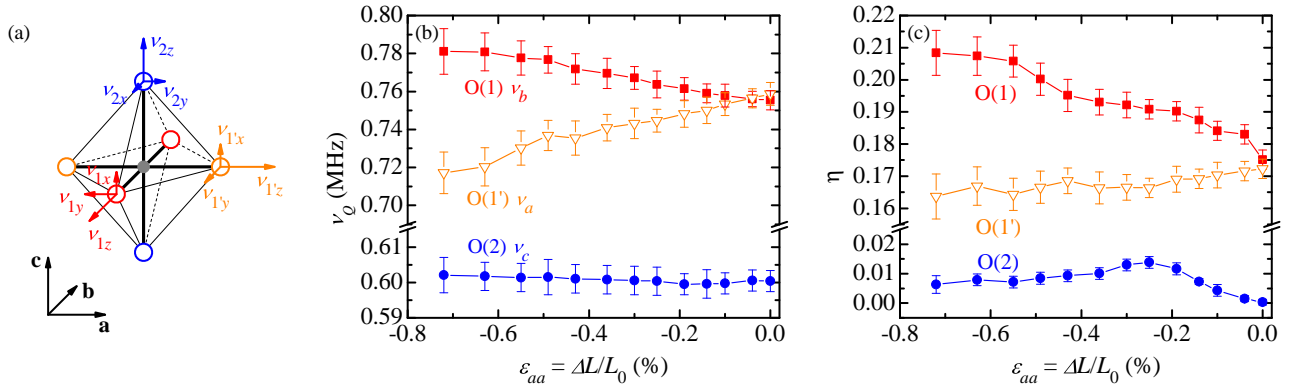


FIG. S3. (a) Schematic sketch of EFG tensors at O sites. The principle component ν_z is along the Ru-O bond, and the length of the arrows characterizes the magnitude of ν_i ($i=x,y,z$). (b) and (c) show strain dependence of $\nu_Q(=\nu_z)$ and asymmetry parameter η , respectively.

Theoretically, ν_Q usually consists of two contributions: point charge (ionic) of other ions and on-site hole in O p orbitals,

$$\nu_Q = \nu_Q^{ionic} + \nu_Q^{hole}, \quad (\text{S4})$$

we shall consider them separately. The ionic term can be calculated by (in SI unit):

$$\nu_Q^{ionic}[\text{Hz}] = \frac{1}{4\pi\epsilon_0} \frac{3eQV_{zz}^{ionic}}{2I(2I-1)\hbar} (1 - \gamma_\infty), \quad (\text{S5})$$

where nuclear spin $I=5/2$, quadrupole moment $Q=-0.026 \times 10^{-28} \text{ m}^2$, and γ_∞ refers to the Sternheimer antishielding factor which accounts for the contribution from the distortion of the O ion both by the local EFG and by the quadrupolar field of the nucleus[49]. This antishielding factor turns out to be not important in Sr_2RuO_4 , much weaker than in cuprates[49], we therefore ignore it hereafter. V_{zz}^{ionic} can be calculated with the crystalline lattice parameters $a=b=3.8603 \text{ \AA}$, and $c=12.729 \text{ \AA}$, and coordinates of the ions Sr^{2+} (0.5, 0.5, 0.1468), Ru^{4+} (0, 0, 0), $\text{O}(1)^{2-}$ (0.5, 0, 0) and $\text{O}(2)^{2-}$ (0, 0, 0.1619)[50].

The on-site hole contribution ν_Q^{hole} is proportional to the hole content (n) in each O orbitals, and the latter can be obtained from DFT calculations by integrating the partial density of states up to Fermi energy, viz.

$$2 - n = \int_{-\infty}^{E_F} N(E) dE. \quad (\text{S6})$$

The variation of n for each O orbitals are displayed in Fig. S4.

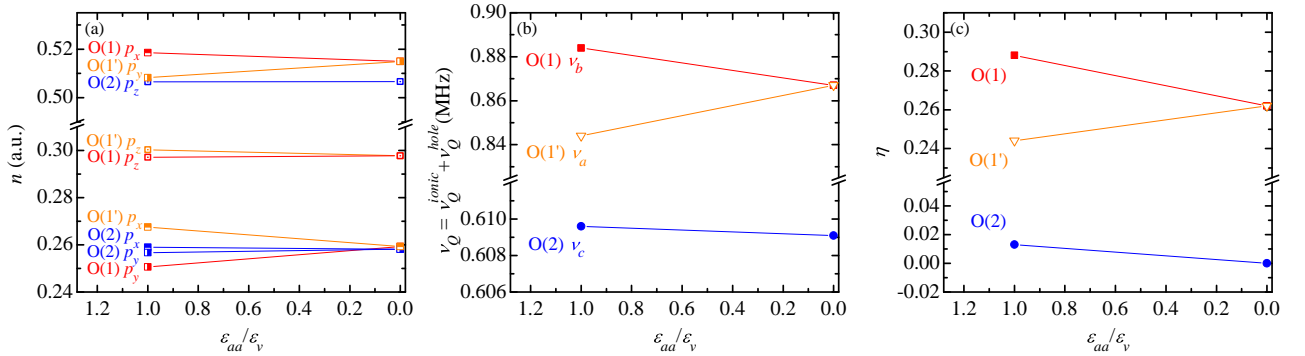


FIG. S4. (a) Comparison of hole content of O orbitals for $\epsilon_{aa}=0$ and ϵ_v where vHS is realized theoretically. (b) and (c) display calculated quadrupolar frequency (ν_Q) and asymmetry parameter (η) as a function of ϵ_{aa} , respectively.

Taking $\text{O}(1) p_x$ orbital as an example, the yielded quadrupolar frequencies are $(\nu_a, \nu_b, \nu_c)_{1,p_x} = n_{1,p_x} (q_{xa}, q_{xb}, q_{xc})$, where the ratios $q_{xa} = -2q_{xb} = -2q_{xc} = 2.452 \text{ MHz}$ for ^{17}O according to previous reports on cuprates[51]. The total quadrupolar frequency should be the sum of the contributions from all the three p orbitals for each O site.

The calculated quadrupolar frequencies ν_Q and the associated asymmetry parameter η are shown in Fig. S4b and c, respectively.

Comparison can be made for ν_Q and η between measured (Fig. S3) and calculated (Fig. S4) results. Regardless of some difference in magnitude, agreement between experiment and theory in the evolution trend upon strain effect is striking at both ν_Q and η .

SM III: Spin-lattice relaxation rate

Additional evidence for vHS comes from the measurements of the spin-lattice relaxation rate $[T_1T]^{-1}$ as shown in Fig. S5. The $[T_1T]^{-1}$ is recorded for the central transition of the $\text{O}(1)$ site and for field $\mathbf{B} \parallel \mathbf{b}$. As a means to extract the strain dependence of the relaxation rate in a minimum of measurement time, the recovery curves at high ($\epsilon_{aa} = \epsilon_v$) and low strain ($\epsilon_{aa} = 0$) were established to follow the appropriate form for spin $I=5/2$, and dominantly magnetic relaxation governing selective irradiation of the central transition. Between these endpoints, a single recovery was recorded, with short delay time selected prior to application of the echo read sequence, so that the relaxation rate could be inferred from the recorded signal amplitude.

As shown in Fig. S5, the relaxation is maximum at the strain where the shifts are extremal, consistent with the vHS-tuning scenario. Although only a narrow temperature range is covered, a temperature dependence is clearly

evident in the inset, where the behavior is contrasted to the zero strain results of Ref. [33]. The variation could originate partially or entirely from proximity to the vHs, with the remainder related to correlations. Note that the singularity in two dimensions scales as $\ln(t/T)$, with t the relevant hopping integral, and its effect on thermodynamic properties is rapidly diminished due to thermal broadening of the Fermi function.

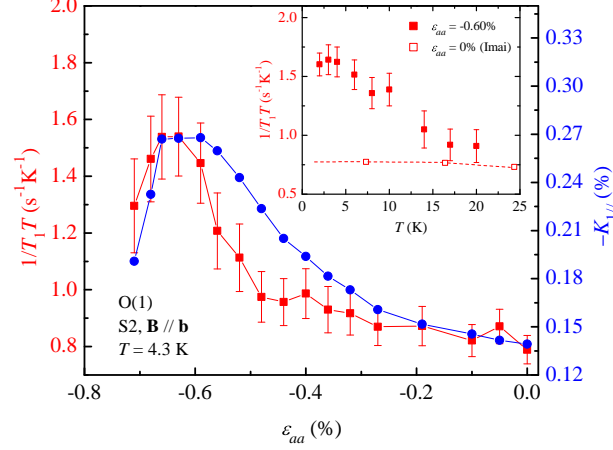


FIG. S5. Magnetization recovery $[T_1T]^{-1}$ of central transition for O(1) site as function of strain ϵ_{aa} , recorded at $T=4.3$ K and with magnetic field aligned with \mathbf{b} -axis. The inset shows a variation with temperature.

SM IV: Comments on the ^{17}O NMR shifts for $\mathbf{B} \parallel \mathbf{c}$

In the main text, the NMR Knight shifts for $\mathbf{B} \parallel \mathbf{c}$ were not closely examined. In part, this is because of an apparently reduced sensitivity to the vHs. In particular, for all strains $|\epsilon_{aa}| < |\epsilon_v|$, the central transition for the O(1,1') sites are only weakly changing and remain unresolved, indicating cancellation effects of contributions to the total shifts. Large changes *are* observed for $|\epsilon_{aa}| > |\epsilon_v|$, where large drops in spin susceptibility and severe line-broadening are qualitatively consistent with inhomogeneous strain within the measured sample volume and an accompanying amplified sensitivity to the inequivalent environments.

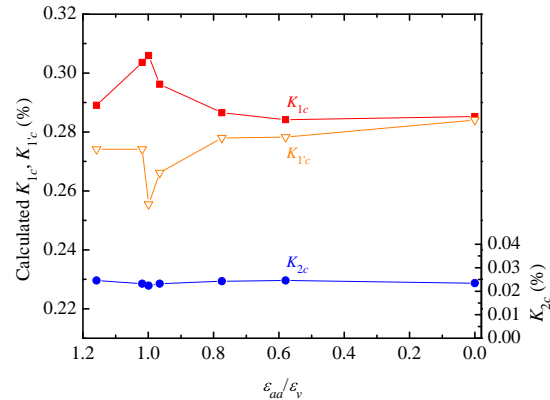


FIG. S6. Calculated total Knight shift for $\mathbf{H} \parallel \mathbf{c}$ for the three sites, O(1), O(1') and O(2). Some discussion of the disparities between these results and what is observed experimentally is included in the main text.

In the DFT calculations for the same quantities, K_{2c} does show essentially full cancellation of the DOS effects, as shown in Fig. S6. On the other hand, both K_{1c} and $K_{1'c}$ appear quite sensitive to the vHs, and, interestingly, in both Fermi and orbital terms. As discussed in the main text, there are two mechanisms by which O electrons can acquire an orbital moment: directly induced by the external field, and via spin-orbit coupling to the induced spin

moment. Our calculations show the former effect in K_{1c} and $K_{1'c}$ to be strong, and *opposite in sign to the spin mechanism*. In the raw calculations the amplitude of the orbital shifts is too small to ensure a full cancellation, but, as discussed in the main text, spin-orbit effects may be considerably enhanced by correlation (Ref. [43]). Assuming a semiphenomenological approach, we plot in Fig. S6 the sum of all contributions to K_{1c} and $K_{1'c}$, *multiplying the orbital part by a factor of four*, without adding any van Vleck constant. The result still show a small split between K_{1c} and $K_{1'c}$ (albeit smaller than the measured peak widths) and an overall good agreement with the measurements. As we declared in the main text, the NMR spectra for the field parallel to \mathbf{c} require further investigation.